Steady Flow Dynamics during Granular Impact

Abram H. Clark,[1,2] Lou Kondic,[3] and Robert P. Behringer[1]

[1] *Department of Physics & Center for Nonlinear and Complex Systems, Duke University, Durham, North Carolina 27708, USA*

[2] *Department of Mechanical Engineering and Materials Science, Yale University, New Haven, Connecticut 06520, USA*

[3] *Department of Mathematical Sciences, New Jersey Institute of Technology, Newark, New Jersey 07102, USA*

(Dated: October 7, 2015)

We study experimentally and computationally the dynamic flow of granular material during impacts, where intruders strike a collection of disks from above. In the regime where granular force dynamics are much more rapid than the intruder motion, we find that the particle flow near the intruder is proportional to the instantaneous intruder speed; it is essentially constant when normalized by that speed. The granular flow is nearly divergence-free and remains in balance with the intruder despite the latter's rapid deceleration, which may explain similarities between impacts and steady drag experiments. Simulations indicate that this observation is insensitive to grain properties, including friction, although friction has a substantial effect on the intruder dynamics (e.g., the final penetration depth). The separation of time scales between grain and intruder dynamics explains the insensitivity to grain properties. Our results suggest that other time-dependent granular flows may have similar dependence on the rate of external driving, if a comparable separation of time scales applies.

PACS numbers: 47.57.Gc, 81.05.Rm, 78.20.hb
Keywords: Granular materials, Granular flow, Impact

What is the nature of force transmission and particle flow during intrusion into granular material? This question is fundamental to a general understanding of dense granular flow, and a complete description would be useful in many natural and industrial phenomena. There are two common variations of this problem: an intruder that is dragged through a granular medium at a fixed speed, and impact, where an intruder strikes the surface of a granular bed and is decelerated. In the case of constant velocity, the force exerted by the grains on the intruder is rate-independent for low velocities near the quasi-static regime [1–5] and then dominated by a velocity-squared drag force for larger velocities [6, 7].

The case of impact is anything but static in time, as the intruder strikes a bed of grains and slows to a stop in a fraction of a second. The highly transient nature of impact seemingly presents a major obstacle to a simple connection to the constant velocity case (or, more generally, well developed granular flows). However, previous studies [8–15], with moderate impact speeds of $v_0 < 10$ m/s, often find drag forces that are similar to constant velocity drag: a rate-independent term, which increases with depth, and a velocity-squared term with a coefficient that is nearly independent of the intruder dynamics. However, we note that the granular media in these studies is typically sand or glass beads, where typical force transmission speeds $v_f > 100$ m/s, such that $v_0 \ll v_f$. So, while the granular flow during these impacts is never well developed (due to rapid intruder deceleration), there is a large separation between times scales for force transmission and intruder motion.

To explicitly explore how these fast force dynamics relate to the intruder motion, we have previously studied granular impact experimentally using high-speed imaging of intruder impacts into beds of photoelastic disks [13–16]. These studies showed that the deceleration is dominated by large fluctuations in space and time in the form of quasi-random collisions with networks of particles. On longer time scales, these fluctuating forces average to the rate-independent and velocity-squared drag forces studied previously. When $v_0 \ll v_f$, the fast force transmission speeds mean that the material responds quickly to the advancing intruder, and the quasi-random collisions with force-chain-like structures [15] yield a velocity-squared drag force with a drag coefficient that is nearly constant over the intruder trajectory [14, 15]. However, the grain-scale force picture and the subsequent intruder dynamics change drastically when the intruder speed becomes similar to granular force transmission speeds [16].

To complement previous work on force dynamics, we present experimental and computational results on the flow of a 2D granular material around circular intruders that are normally incident on a free granular bed from above at speeds $v_0 \leq 6$ m/s. The experiments are carried out using the protocol described in [13–16], and outlined in Supplemental Materials (SM) for completeness. To explore the influence of the interaction force between the granular particles on the results, simulations are carried out using both linear and nonlinear (Hertzian) force models.

The main result from both experiments and simulations is that an intruder remains in a dynamic steady-state with the flow of the granular material for essentially the entire trajectory, despite the highly transient

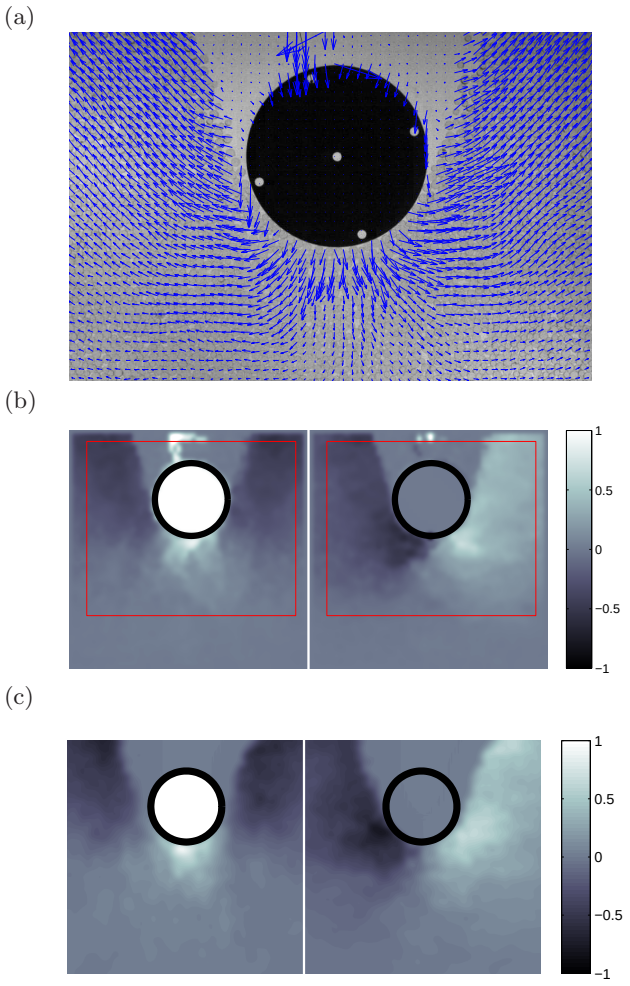

FIG. 1. (color online.) (a) PIV flow field for a circular intruder with radius $R = 6.35$ cm at a particular frame. (b) Vertical and horizontal components of the spatially smoothed PIV flow field from experiment, normalized by the instantaneous intruder velocity ($v = 3.05$ m/s). The left panel shows the normalized vertical velocity, u_z/v, with downward as positive, and the right panel shows the horizontal velocity, u_x/v, with rightward as positive. The white color in the intruder in the left panel denotes its downward motion. The red box encloses the region used to obtain the steady-state velocity field, which will move along with the intruder. (c) The instantaneous flow fields, u_z/v and u_x/v, at a particular time from simulations with Hertzian, frictional interactions between grains.

nature of this process. By dynamic equilibrium, we mean that as the intruder moves through the granular material, the flow field near the intruder scales linearly with the instantaneous intruder speed, even as the intruder decelerates rapidly. Since $v_0 \ll v_f$, the force dynamics are much faster than intruder motion, and forces propagate and relax fast enough that the motion of grains near the intruder is essentially incompressible and always scales linearly with the intruder's speed.

The techniques for the accompanying simulations are described in detail in SM, and here we provide just an overview. The particle and the intruder are modeled as inelastic, frictional disks, and only circular intruders are considered. The container walls are modeled by a layer of stationary strongly inelastic particles. The number of particles and their size distribution are matched to the experiments, as are the material parameters (friction and restitution coefficient, Young modulus, Poisson ratio). The simulations implement a standard Cundall-Strack model to describe frictional interactions, although some simulations are carried out without friction. The simulations with a linear force model are carried out as described in [17]; in particular, the force constant needed to compute the normal force between the particles is based on the requirement that the binary contact times agree with the nonlinear force law found experimentally (see [18]). The nonlinear simulations use a Hertzian interaction potential, with the force constant computed by fitting the experimental data obtained by statically compressing granular particles (see [16]).

Experimentally, the flow fields are calculated using particle image velocimetry (PIV) [19], which analyzes successive pairs of frames from high-speed movies to estimate the local flow field. This returns estimates of the local displacement on a grid, as shown in Fig. 1. Results from PIV (for experiments) or actual particle positions and velocities (for simulations) can then be coarse-grained [20–22], as shown in Fig. 1(b) and (c), to give a continuum flow field $\mathbf{u}(\mathbf{x}, t)$, where $\mathbf{x}$ represents spatial coordinates in the lab frame. The vertical component, $u_z(\mathbf{x}, t)$ (with downward being positive z), and the horizontal component, $u_x(\mathbf{x}, t)$ (with rightward being positive x) components of the flow field at are shown in Fig. 1(b) for experiments. The grid size used for the PIV algorithm is approximately the same size as a single particle, so the particle-scale fluctuations in the velocity fields still persist. To compare simulation results to PIV, we use a coarse-grained momentum field normalized by a typical mass density, as shown in Fig. 1(c) (see SM for details).

In both experiments and simulations, we find that

$$\mathbf{u}(\mathbf{x}, t) = v(t) \left[\mathbf{A}(\mathbf{x} - \mathbf{x}_0) + \mathbf{A}'(\mathbf{x} - \mathbf{x}_0, t)\right], \qquad (1)$$

where $v(t)$ is the intruder speed (with motion assumed to be strictly downward), $\mathbf{x}_0(t)$ is the intruder position in the lab frame, $\mathbf{A}$ is the scaled steady-state velocity field, and $\mathbf{A}'$ captures the instantaneous fluctuations in the velocity field. $\mathbf{A}$ is shown in Fig. 2(a) for experiments and in SM for simulations. $\mathbf{A}$ for simulations appears identical to Fig. 2(a), and we quantitatively show that they agree in our analysis below. In each experimental trajectory, we calculate $\mathbf{A}$ by averaging over approximately 300 pairs of frames, sampled at 2333 Hz, using flow-field data inside the red rectangular region marked in Fig. 1(b) at each frame where this rectangular region is entirely in the field of view. $\mathbf{A}$ appears very similar to the instantaneous

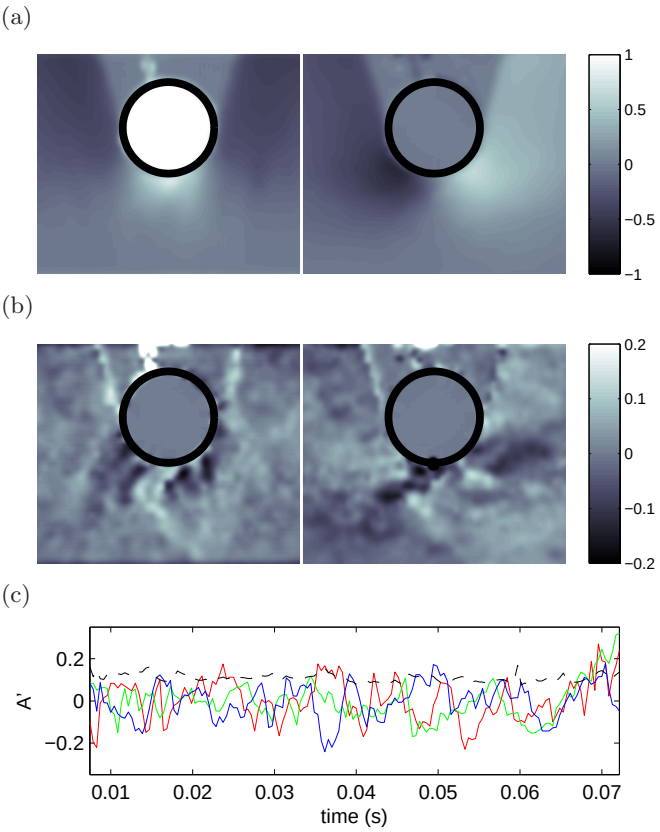

FIG. 2. (color online.) (a) The average flow field, $\mathbf{A}$, from experiments for a circular intruder with radius $R = 6.35$ cm. The left side shows the vertical velocity A_z (down is positive), and the right side shows the horizontal velocity, A_x (right is positive). The white color in the intruder in the left panel denotes its downward motion. (b) The instantaneous fluctuations, $\mathbf{A}'$, in the flow field at a particular frame from experiments for a circular intruder with radius $R = 6.35$ cm, with A'_z on the left and A'_x on the right. (c) Time series of $\mathbf{A}'$, where solid lines (red, blue, and green) are plots of A'_z at three points beneath the intruder. These signals fluctuate around zero with a correlation time of roughly 3 ms. Dashed line is a time series of the root-mean-squared value of $\mathbf{A}'$, which is essentially constant in time. This quantity is computed at each frame in the region directly beneath the intruder, $R < r < 2R$ and $-pi/4 < \theta < \pi/4$, where the fluctuations are most prominent (see SM).

flow fields shown in Fig. 1(b) and (c), but smoother spatially. $\mathbf{A}'$ is determined at each time from the difference between the instantaneous coarse-grained flow field and the average flow field, $\mathbf{A}' = \mathbf{u}/v(t) - \mathbf{A}$. An experimental measurement of $\mathbf{A}'$ at one instant is shown in Fig. 2 (b), which is typical for all times in both simulation and experiment (see SM).

Using numerical derivatives, we find that $\mathbf{A}$ is divergence free within noise, and thus the flow of grains near the intruder is essentially incompressible (see SM). The magnitude $|\mathbf{A}'|$ is always small, Figure 2(c), with $|\mathbf{A}'| < 0.2$ (where a value of 1 would correspond to a local velocity fluctuation of the same size as the intruder speed); it is largest near the leading edge of the intruder and falls off rapidly with increasing distance from the intruder. $\mathbf{A}'$ is statistically stationary in time and decoupled from the intruder dynamics. We also find that $\mathbf{A}'$ is spatially well correlated to gradients in $\mathbf{A}$ [23, 24]; see SM for details. Physically, $\mathbf{A}'$ represents non-affine particle rearrangements as particles are forced to move past each other, as opposed to a systematic evolution related to the intruder motion.

To fit $\mathbf{A}$ to a functional form, it is decomposed into radial and angular components

$$\mathbf{A}(\mathbf{x}) = \hat{\mathbf{r}}\left[\cos\theta - A_r(\mathbf{r})\right] + \hat{\boldsymbol{\theta}}\left[A_\theta(\mathbf{r}) - \sin\theta\right]. \quad (2)$$

Here, $\mathbf{r} = r\hat{\mathbf{r}} + \theta\hat{\boldsymbol{\theta}}$, where $\mathbf{r} = 0$ corresponds to the center of the intruder, θ is measured from the (downward) z-axis. Shifting by $\hat{\mathbf{z}} = \cos\theta\hat{\mathbf{r}} - \sin\theta\hat{\boldsymbol{\theta}}$ corresponds to a transfer from the lab frame to the intruder frame. A_r and A_θ are defined as

$$A_r(\mathbf{r}) = a_r(r)\cos[b_r(r)\theta] \quad (3)$$
$$A_\theta(\mathbf{r}) = a_\theta(r)\sin[b_\theta(r)\theta]. \quad (4)$$

Seguin et al. [4, 5] used a similar form to describe quasistatic granular flow around downward-moving circular obstacles, but with $b_r = b_\theta = 1$, since, in their quasistatic case, the flow was symmetric ahead of and behind the intruder. Here, we consider fits only to the half-space in front of the intruder. Sample fits at particular values of r are shown in Fig. 3. Far away, all four fit parameters should approach 1, corresponding to no grain motion.

Figure 3 shows $a_r(r)$, $b_r(r)$, $a_\theta(r)$, and $b_\theta(r)$ for different circular-nosed intruders with radii $R = 3.18$, 4.65, 6.35, and 10.15 cm. The intruder with $R = 4.65$ cm is an ogive, with a circular nose and rectangular tail; however, the particles are never in contact with the tail, so that its presence is irrelevant, aside from increasing the area of the intruder and therefore its effective mass. The fit parameters for each intruder appear similar when rescaled by R, with secondary dependencies on the ratio $\rho_{\rm int}/\rho_g$ of intruder to grain mass density and on the ratio d/R of grain size to intruder radius, where $d \approx 5$ mm. a_r and b_r decay roughly exponentially to their far-field values as $a_r \propto \exp(-R/\xi_{a_r})$ and $b_r \propto \exp(-r/\xi_{b_r})$, with $0.25R < \xi_{a_r} < 0.7R$ and $\xi_{b_r} \approx 1.85R$. This localization and exponential spatial decay is also common in dense granular flows that are driven by a boundary (e.g., Refs. [4, 5, 24], and many others).

To test sensitivity to the grain-grain force law, we perform simulations with frictional Hertzian, frictional linear, and frictionless linear force interactions between the particles. Figure 4 shows a comparison between the fit of experimental and computational data to Eqs. (2)-(4) for a single size intruder; this is typical for all sizes, as we show in SM. We find surprisingly good agreement for all considered force models. Such a good agreement

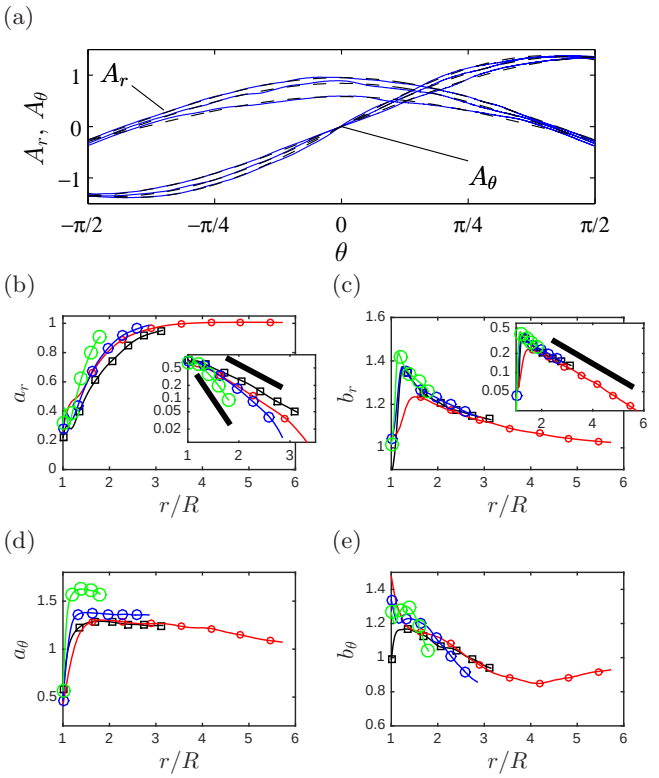

FIG. 3. (color online.) (a) Typical fits of the flow field to the form shown in Eq. (2) for one intruder (radius $R = 3.18$ cm) at $r = 1.5R$, $2R$, and $3R$, where $r = R$ corresponds to the intruder boundary. Solid blue lines are data, and dashed black lines are fits of the form shown in Eq. (2). (b)-(e) A comparison of the fit parameters—$a_r(r), b_r(r), a_\theta(r), b_\theta(r)$—for circular intruders with $R = 3.18$ cm (red circles) $R = 6.35$ cm (blue circles), $R = 10.15$ cm (green circles), as well as the circular nosed intruder with $R = 4.65$ cm and a rectangular tail (black squares). The inset of (b) show semi-log plots of $1 - a_r(r)$ versus r/R; thick black reference lines show exponential decay with decay lengths of $0.7R$ (upper) and $0.25R$ (lower). The inset of (c) shows semi-log plots of $b_r(r) - 1$ versus r/R; thick black reference line shows exponential decay with decay length $1.85R$.

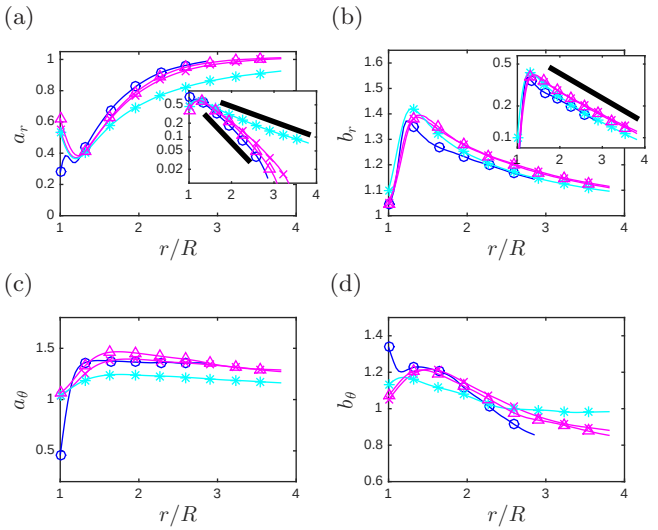

FIG. 4. (color online.) Comparison of the parameters $a_r(r)$, $b_r(r)$, $a_r(r)$, and $a_\theta(r)$ between experimental data (blue circles) from Fig. 3 and simulations using frictional linear (magenta crosses), frictional Hertzian (magenta triangles) and frictionless linear (light blue asterisks) interactions, all under the same conditions with $R = 6.35$ cm. Insets of (a) and (b) show semi-log plots of $1 - a_r(r)$ and $b_r(r) - 1$, respectively, versus r/R. Thick black reference lines show exponential decay with decay lengths in the (a) of $1.3R$ (upper) and $0.45R$ (lower), and in (b) of $1.85R$.

shows that in the present regime, the details of the force model are not crucial for the response of granular material to impact. However, we note that frictional forces still play an important role in determining dynamics of the intruder; in particular, without friction, the final penetration depth is almost 50% larger than when friction is present (see SM). The functional form of the normal forces between the particles (linear versus nonlinear) however does not appear to be important. We attribute this finding to the fact that we consider the regime such that $v_0 \ll v_f$; the functional form of the force model becomes important when this condition is not satisfied [16, 25].

These results provide several important physical insights. First, while the force response here, where grain forces are imbalanced and the force response scales quadratically with driving rate, clearly distinguishes impact from quasi-static processes, where grain forces are nearly balanced and rate-independent, we find that particle motion scales linearly with driving speed, as in quasi-static systems. This is made possible in both cases by the large difference between the force transmission speed v_f and driving speed v_0, as is common in impact flows involving sand or glass beads. Somewhat surprisingly, although final penetration depth is strongly influenced by frictional interactions, the granular flow itself appears relatively insensitive to the presence of friction [15, 26]. In addition, the finding from simulations that the details of the grain-grain force law (e.g., linear versus Hertzian) are not crucial for obtaining accurate grain motion is consistent with work by Campbell [25] on simulations of shear flows. This suggests that other well developed granular flows, such as those described in the context of $\mu(I)$ rheology [27–29] models, may also fall into the same class as the present impact flows, since typical macroscopic speeds v_0 satisfy $v_0 \ll v_f$. Conversely, it is possible that models such as $\mu(I)$ could be extended to processes such as granular impact [30], where the flow is transient, provided $v_0 \ll v_f$. We note that the response of the granular material to impact when the condition $v_0 \ll v_f$ is not satisfied is significantly different [16].

This work has been supported by the U.S. DTRA under Grant No. HDTRA1-10-0021, by NASA grant NNX15AD38G, and by NSF Grant DMR-1206351.

[1] R. Albert, M. A. Pfeifer, A.-L. Barabási, and P. Schiffer, Phys. Rev. Lett. **82**, 205 (1999).

[2] I. Albert, J. G. Sample, A. J. Morss, S. Rajagopalan, A.-L. Barabási, and P. Schiffer, Phys. Rev. E **64**, 061303 (2001).

[3] J. Geng and R. P. Behringer, Phys. Rev. E **71**, 011302 (2005).

[4] A. Seguin, Y. Bertho, P. Gondret, and J. Crassous, Phys. Rev. Lett. **107**, 048001 (2011).

[5] A. Seguin, Y. Bertho, F. Martinez, J. Crassous, and P. Gondret, Phys. Rev. E **87**, 012201 (2013).

[6] Y. Takehara, S. Fujimoto, and K. Okumura, EPL **92**, 44003 (2010).

[7] Y. Takehara and K. Okumura, Phys. Rev. Lett. **112**, 148001 (2014).

[8] W. A. Allen, E. B. Mayfield, and H. L. Morrison, Journal of Applied Physics **28**, 370 (1957).

[9] M. Forrestal and V. Luk, International Journal of Impact Engineering **12**, 427 (1992).

[10] H. Katsuragi and D. J. Durian, **3**, 420 (2007).

[11] D. I. Goldman and P. Umbanhowar, Phys. Rev. E **77**, 021308 (2008).

[12] P. Umbanhowar and D. I. Goldman, Phys. Rev. E **82**, 010301 (2010).

[13] A. H. Clark, L. Kondic, and R. P. Behringer, Phys. Rev. Lett. **109**, 238302 (2012).

[14] A. H. Clark and R. P. Behringer, EPL (Europhysics Letters) **101**, 64001 (2013).

[15] A. H. Clark, A. J. Petersen, and R. P. Behringer, Phys. Rev. E **89**, 012201 (2014).

[16] A. H. Clark, A. J. Petersen, L. Kondic, and R. P. Behringer, Phys. Rev. Lett. **114**, 144502 (2015).

[17] L. Kondic, X. Fang, W. Losert, C. O'Hern, and R. Behringer, Phys. Rev. E **85**, 011305 (2012).

[18] L. Kondic, Phys. Rev. E **60**, 751 (1999).

[19] I. Grant, Proceedings of the Institution of Mechanical Engineers, Par http://pic.sagepub.com/content/211/1/55.full.pdf+html.

[20] I. Goldhirsch and C. Goldenberg, The European Physical Journal E **9**, 245 (2002).

[21] I. Goldhirsch, Granular Matter **12**, 239 (2010).

[22] A. H. Clark, P. Mort, and R. P. Behringer, Granular Matter **14**, 283 (2012).

[23] N. Menon and D. J. Durian, Science **275**, 1920 (1997), http://www.sciencemag.org/content/275/5308/1920.full.pdf.

[24] W. Losert, L. Bocquet, T. C. Lubensky, and J. P. Gollub, Phys. Rev. Lett. **85**, 1428 (2000).

[25] C. S. Campbell, Journal of Fluid Mechanics **465**, 261 (2002).

[26] A. Seguin, Y. Bertho, P. Gondret, and J. Crassous, EPL (Europhysics Letters) **88**, 44002 (2009).

[27] F. da Cruz, S. Emam, M. Prochnow, J.-N. Roux, and F. m. c. Chevoir, Phys. Rev. E **72**, 021309 (2005).

[28] P. Jop, Y. Forterre, and O. Pouliquen, Nature **441**, 727 (2006).

[29] K. Kamrin and G. Koval, Phys. Rev. Lett. **108**, 178301 (2012).

[30] S. Dunatunga and K. Kamrin, Journal of Fluid Mechanics **779**, 483 (2015).